M. A. Panzer
Department of Mechanical Engineering,
Stanford University,
Room 101, Building 530,
440 Escondido Mall,
Stanford, CA 94305
e-mail: mpanzer@stanford.edu

G. Zhang

D. Mann

Department of Chemistry,
Stanford University,
Room 125, William Keck Science Building,
Stanford, CA 94305

X. Hu
Intel Corporation,
5000 W Chandler Blvd.,
Chandler, AZ 85226

E. Pop
Department of Electrical and Computer Engineering,
University of Illinois at Urbana-Champaign,
Urbana, IL 61801-2918

H. Dai
Department of Chemistry,
Stanford University,
Room 125, William Keck Science Building,
Stanford, CA 94305

K. E. Goodson
Department of Mechanical Engineering,
Stanford University,
Room 101, Building 530,
440 Escondido Mall,
Stanford, CA 94305

Thermal Properties of Metal-Coated Vertically Aligned Single-Wall Nanotube Arrays

Owing to their high thermal conductivities, carbon nanotubes (CNTs) are promising for use in advanced thermal interface materials. While there has been much previous research on the properties of isolated CNTs, there are few thermal data for aligned films of single wall nanotubes. Furthermore, such data for nanotube films do not separate volume from interface thermal resistances. This paper uses a thermoreflectance technique to measure the volumetric heat capacity and thermal interface resistance and to place a lower bound on the internal volume resistance of a vertically aligned single wall CNT array capped with an aluminum film and palladium adhesion layer. The total thermal resistance of the structure, including volume and interface contributions, is $12\ m^2\ K\ MW^{-1}$. *The data show that the top and bottom interfaces of the CNT array strongly reduce its effective vertical thermal conductivity. A low measured value for the effective volumetric heat capacity of the CNT array shows that only a small volume fraction of the CNTs participate in thermal transport by bridging the two interfaces. A thermal model of transport in the array exploits the volumetric heat capacity to extract an individual CNT-metal contact resistance of* $10\ m^2\ K^1\ GW^{-1}$ *(based on the annular area* $A_a=\pi db$*), which is equivalent to the volume resistance of* 14 nm *of thermal* SiO_2. *This work strongly indicates that increasing the fraction of CNT-metal contacts can reduce the total thermal resistance below* $1\ m^2\ K\ MW^{-1}$. [DOI: 10.1115/1.2885159]

Keywords: vertically aligned carbon nanotubes, thermal interface resistance, thermoreflectance thermometry, thermal interface material, single wall carbon nanotube

Introduction

The outstanding thermal properties of carbon nanotubes (CNTs), particularly their extraordinary thermal conduction properties, have generated considerable interest and research activity. Past work investigated the thermal properties of individual single wall nanotubes [1–9], multiwalled nanotubes [10,11], bulk films of nanotubes [12,13], nanotube composites [14–19], and aligned arrays of mulitwalled nanotubes [20–22]. A very promising application is the use of vertically aligned arrays of CNTs as thermal interface materials (TIMs) for electronic systems. TIMs require a high thermal conductivity, a low thermal interface resistance with the adjacent microprocessor and heat sink, as well as significant mechanical compliance to help minimize the impact of mismatched thermal expansion coefficients. Many TIM materials, such as particle-filled organics and related composites, offer excellent mechanical compliance with the penalty of relatively poor thermal conductivity. Other materials, such as alloyed metals and eutectics, offer relatively good thermal conduction properties with the penalty of poor mechanical compliance and reliability concerns related to thermal cycling. CNT films, which consist of many flexible nanotubes, may eventually provide both high thermal conductivity and lateral compliance, a truly unique combination of properties that could be very attractive for interfaces in electronic systems. However, past work has suggested that the thermal performance of CNT films is impeded by high thermal interface resistances, indicating that more detailed measurements and improved fabrication methods will be needed.

The thermal conductivity of individual single wall CNTs (SWNTs) and multiwall CNTs (MWNTs) has been the subject of recent theoretical and experimental research activity. Experimental and molecular dynamic studies have yielded room temperature

Contributed by the Heat Transfer Division of ASME for publication in the JOURNAL OF HEAT TRANSFER. Manuscript received October 26, 2006; final manuscript received September 17, 2007; published online April 8, 2008. Review conducted by Suresh V. Garimella.

thermal conductivities of individual SWNTs in the range of 2500–6600 W m^{-1} K^{-1} [1–4]. For MWNTs, past research yielded similar values in the range of 2000–3000 W m^{-1} K^{-1} [10,11]. Theoretical works predict that ballistic transport effects, interface scattering, and modification to the phonon modes in submicron length individual SWNTs tend to reduce their thermal conductivity to values below 350 W m^{-1} K^{-1} [5–9]. Likewise, measurements of bulk CNT films yielded lower thermal conductivities in the range of 20–200 W m^{-1} K^{-1} [12,13]. The discrepancy between the thermal conductivities of individual CNTs and their value in bulk films can be attributed to various effects. In particular, tube-tube contact, tube-matrix contact, and an increased defect density due to bulk film preparation methods may reduce the phonon mean free path compared to its value in individual tubes. The tube-matrix contact has been the focus of several studies [14,15,23]. Furthermore, the defined area of heat flow through the nanoscale geometries of both the individual constituent tubes and the film itself is often ambiguous and subject to variation, directly influencing the reported values of CNT thermal conductivities. This problem is particularly acute with MWNT films, which often exhibit significant variations in individual tube cross-sectional areas within a film.

Although the bulk thermal performance of CNT films falls short of the theoretical expectations, the use of CNTs as fillers in advanced TIMs and in nanostructured composite films greatly improves the thermal performance of the material. A CNT volume fraction of 1% showed an increase in the effective thermal conductivity of 2.5 in silicon oil [16] and 125% for epoxy [17]. Similarly, by suspending SWNTs randomly oriented in a polymethyl methacrylate (PMMA) composite, Guthy et al. [18] measured a thermal conductivity enhancement that saturated at 240% for 6 vol % SWNTs. Additionally, Hu et al. [19] combined CNTs with traditional nickel fillers, creating a sevenfold increase in the effective thermal conductivity of the base fluid, twice that of a nickel nanoparticle filler alone.

Other investigations showed that creating vertically aligned CNT films better utilizes the outstanding thermal conductivity of individual CNTs. Using the 3ω method, Hu et al. [20] measured the room temperature thermal conductivity of a 13 μm thick vertically aligned MWNT film grown on silicon to be 75 W m^{-1} K^{-1}, which outperforms that of randomly oriented tube samples. However, the total thermal resistance of the aligned CNT TIM was found to be 16 m^2 K MW^{-1}, which still falls well short of theoretical expectations. Yang et al. [21] performed a similar measurement of MWNT films using a thermoreflectance technique and found the effective thermal conductivities to be around 15 W m^{-1} K^{-1}, with total thermal resistances falling in the range of 0.8–2.9 m^2 K MW^{-1}. Even accounting for porosity effects, the reduced performance of these aligned MWNT films indicates that the thermal boundary resistance between the CNT and the substrate is the problem.

Much of the variation observed in the previous data can be attributed to the impact of thermal interface resistances in CNT films. The relative importance of thermal interface resistance in CNT based TIMs was recently confirmed by Tong et al. [22] in a transient phase sensitive photothermal measurement of an aligned MWNT TIM. The TIM was formed by dry adhesion of a 7 μm thick MWNT array, grown on a Si wafer, to a glass plate. The total resistance of the TIM was measured to be 12 m^2 K MW^{-1}, which was dominated by the dry glass interface resistance of 11 m^2 K MW^{-1}. The importance of the thermal interface resistance in CNT arrays motivates its further study as well as the need for metrology that focuses on this property.

In this paper, we measure and model the room temperature thermal properties of a 28 μm thick metal-coated vertically aligned SWNT film using a nanosecond thermoreflectance technique. Our objective is to extract, model, and illuminate the governing physics of the interface resistance. A 6 ns heating pulse from a frequency doubled Q-switched Nd:YAG (yttrium aluminum garnet) laser generates a transient temperature field in the metalized film, and the combination of submicrosecond laser-reflectance thermometry and effective medium modeling extracts the vertical distribution of area-averaged thermal properties in the system. The transient time scales of the measurement provide a means to separate the relative importance of thermal resistance within the film from those of the film boundaries. Isolating the thermal boundary resistances and measurement of the CNT volumetric heat capacity enables an understanding of the low measured effective thermal conductivity of the aligned SWNTs. This study provides insight into the physical mechanisms governing the thermal resistance in aligned CNT films, which will enable innovations in fabrication technology to reduce the total thermal resistance and lead to promising interface materials.

Experimental Method

Sample Preparation. The aligned SWNT sample was prepared as follows. First, an iron film 1–2 Å thick is deposited using electron beam evaporation on a 10 nm thick thermal oxide layer grown on the silicon substrate. Subsequent annealing in oxygen at 550°C produced a monolayer of ~1.3 nm diameter iron clusters to act as catalysts for the CNT growth. The CNT synthesis was carried out in a coupled-rf chemical vapor deposition (CVD) plasma system with a mixture of methane, hydrogen, and oxygen. Additional details of the CNT growth process are discussed in Ref. [24].

The scanning electron microscopy (SEM) profile of the sample in Fig. 1(*a*) shows that the tube length is 28 μm. Raman data [24] indicate that the SWNT diameter d is in the range of 1–2 nm, with the average being close to the average catalyst diameter of ~1.3 nm. Since the SWNT growth conditions yield approximately one nanotube per iron catalyst cluster [24], we estimate the SWNT number density to be 8.7×10^{16} m^{-2} based on the thickness of the deposited catalyst layer and cluster diameter after annealing. This number density corresponds to a volume fraction of ~12% based on the average SWNT annular area $A_a=\pi db$, where we use an average diameter of $d=1.3$ nm and $b=3.4$ Å, the thickness of a graphene plane. A premetalization topographic profile, produced by scanning atomic force microscopy (AFM), of the top of the CNT film is shown in Fig. 1(*b*) and indicates that the rms roughness of the film is ~60 nm.

Prior to the evaporation of the 160 nm thick aluminum film, an initial evaporation of a 20 nm thick palladium film on the exposed CNT ends enhances the metal-CNT contact interface. A SEM image (Fig. 1(*c*)) of the top of the metal film taken after deposition shows that the surface is rough and porous on the submicron scale. The potential effects of the film porosity on its optical properties will be considered in the following section.

Experimental Setup and Procedure. The thermal properties of the metallized SWNT film are measured using a thermoreflectance technique in which a high power pump laser induces a transient temperature field in the metal film. The reflected intensity of a second low power cw probe laser, being proportional to the metal temperature, provides a dynamic measurement of the temperature response of the metal film. The thermoreflectance technique has been used in the nanosecond regime to characterize the thermal properties of thin films [21,25,26] in the picosecond regime to measure both the thermal properties of thin films and their interfaces [27–29] and in the femtosecond regime to measure electron and phonon processes [30,31].

Figure 2 is a schematic of the optical path and experimental configuration along with a schematic of the sample geometry. A 650 MHz photodiode and amplifier measure the reflected intensity of a 10 mW diode laser at 637 nm wavelength, which is focused on the sample with a spot size of approximately 10 μm. The metal film on top of the CNTs is heated using a 10 Hz, 6 ns pulse width Nd:YAG laser, frequency doubled to 532 nm.

The transient metal temperature is measured through the tem-

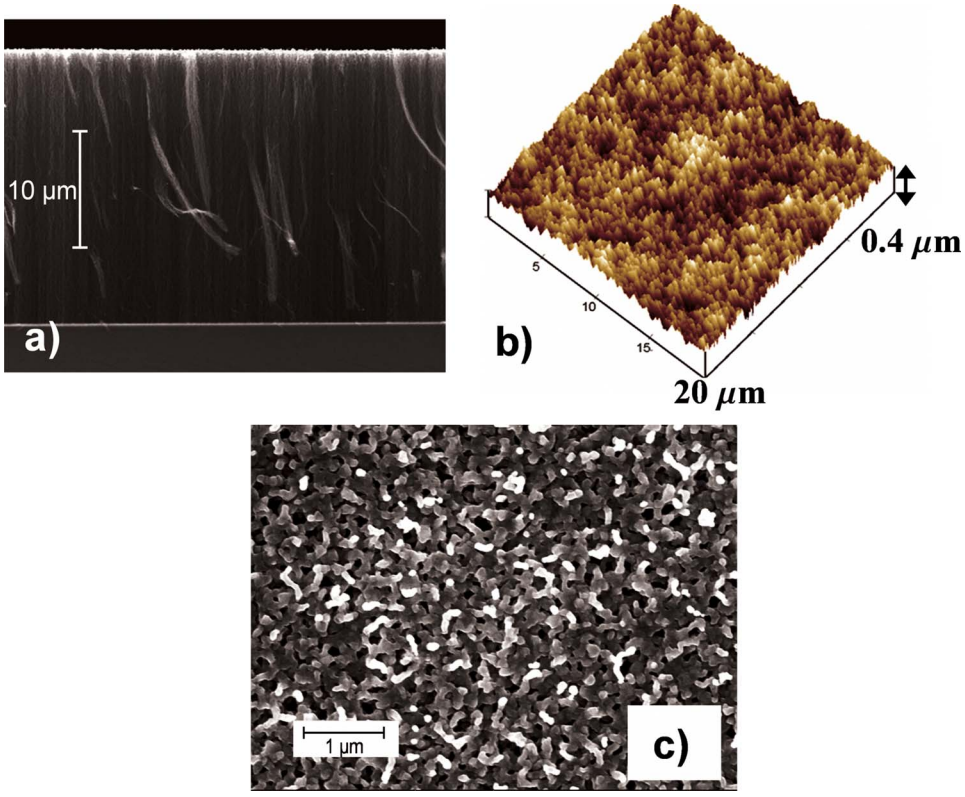

Fig. 1 (*a*) **SEM profile of aligned SWNTs grown on Si—the tube length is 28 μm. The SWNT diameter ranges between 1 nm and 2 nm, with an average of approximately 1.3 nm. (*b*) AFM topographic profile of the top of the CNT film, which indicates that the rms surface roughness is ~60 nm. (*c*) SEM of the top of the metal film after it has been deposited on CNTs. The image shows that the metal film is porous at a scale below 100 nm.**

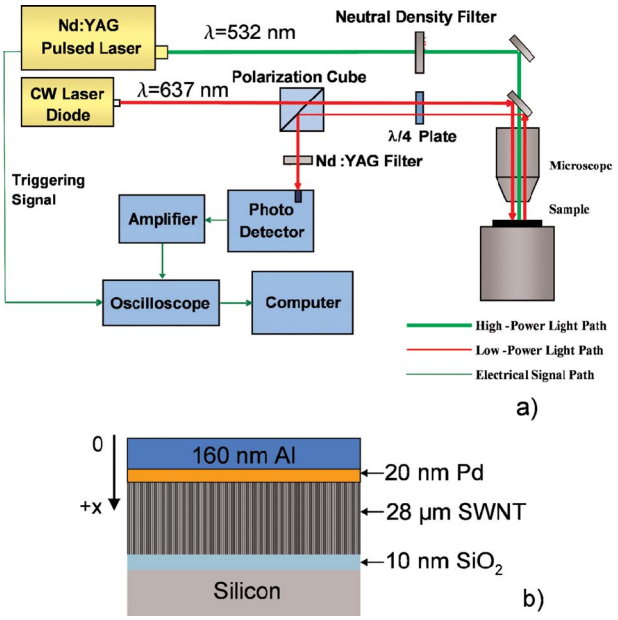

Fig. 2 (*a*) **Schematic of the thermoreflectance thermometry experimental setup including the optical and signal paths. (*b*) Schematic of the sample geometry. The initial deposition of a 20 nm thick layer of palladium on the SWNT ends forms an adhesion layer with the 160 nm thick aluminum film used for thermal reflectance thermometry.**

perature dependence of its dielectric constant [32]. The linearized temperature dependent reflectivity [33], defines the thermoreflectance coefficient C_{tr} as

$$\frac{\Delta R}{R_0} \equiv C_{tr}\Delta T \tag{1}$$

where R_0 is a reference reflectivity and T is the metal temperature.

Since for most metals, C_{tr} is approximately constant [32,34], the reflected probe intensity is proportional to the metal surface temperature.

The surface topography and porous structure of the metalized CNT films pose significant challenges for photothermal diagnostics. Due to porosity, the optical radiation may be absorbed on both the surface of the metal film and in its pores. However, since all thermal diffusion time scales in the aluminum film are subnanosecond and below the temporal resolution of the equipment, it is inconsequential whether the radiation is absorbed strictly on the metal surface or within the pores of the metal layer.

The transmission of optical radiation through the metal may lead to the possibility of energy absorption in the structure underlying the film, complicating the solution to the heat diffusion equations. Data from the image analysis of the SEM image in Fig. 1(*c*) bounds the potential unmetallized regions to less than 5%. The subwavelength of the nature of the pores further reduces the transmitted radiation by a factor of $(r/\lambda)^4$ [35,36], where r is the hole radius yielding a net energy transmission factor less than 5×10^{-4}. Furthermore, the near field radiation is appreciable only within $\sim 4r$ [36] of the hole and is thus much less than the thermal diffusion distance (~ 4 μm) into the CNT film during the laser pulse. These conclusions render the transmission of optical radiation through the metal film insignificant.

The relatively large surface roughness of the metal film

(~100 nm) augments absorption such that care must be taken to avoid damage and delamination. The mechanical compliance, porosity, and mismatched thermal expansion behavior of the metal coating and underlying CNT film may lead to significant temperature induced changes in the surface topography and associated thermoreflectance coefficient. The value of C_{tr} may also be influenced by microstructural changes in the metal film with temperature, which are related to the reflectivity through electron scattering and the plasma frequency.

We address the above concerns about photothermal interaction with the film through a strong reduction in the heating laser fluence and careful verification that C_{tr} is constant and reproducible in the temperature range of the measurement. For different laser powers, the normalized thermal response trace collapsed to a single shape that depends only on the thermal properties within the structure. Furthermore, the amplitude of the peak reflected probe intensity scaled in direct proportion to the pump power. These results indicate that the interaction of the metal with both lasers is linear and reproducible.

Data Extraction Model and Method. To extract the thermal properties of the CNT film, we fit the experimentally measured thermal response to an analytical solution of the heat diffusion equation based on effective area-averaged thermal properties. As long as heat is fully absorbed by the metal layer and is forced to conduct through the CNT film and into the substrate, the solution of the heat diffusion equation using effective area-averaged properties is a fully rigorous mathematical treatment of the physics and does not require knowledge of the CNT volume fraction. Solving the heat diffusion equation reduces to a 1D problem since the diameter of the heating pulse ($d \sim 6$ mm) is much greater than any of the thermal diffusion distances into the structure during the measurement. The governing equation in each layer is

$$\frac{\partial T_j(x,t)}{\partial t} - \alpha_j \frac{\partial^2 T_j(x,t)}{\partial x^2} = 0 \tag{2}$$

where T_j is the temperature and α_i is the thermal diffusivity of the jth material. We solve the 1D heat diffusion equation by transforming Eq. (2) to the frequency domain

$$\frac{\partial^2 \theta_j(\omega,x)}{\partial x^2} + \frac{i\omega}{\alpha_j}\theta_j(\omega,x) = 0 \tag{3}$$

where θ_j is the Fourier transform of the temperature field and which has the general solution

$$\theta_j(\omega,x) = a_j(\omega)e^{i\sqrt{i\omega/\alpha_j}x} + b_j(\omega)e^{-i\sqrt{i\omega/\alpha_j}x} \tag{4}$$

The laser heating is modeled as a heat flux boundary condition on top of the metal film with a Gaussian shaped heat pulse

$$q''_{laser}(t) = -k_{Al}\left.\frac{\partial T_{Al}(t,x)}{\partial x}\right|_0 \tag{5}$$

$$q''_{laser}(t) = \sqrt{\frac{1}{\pi\tau^2}}\rho_{Al}L_{Al}c_{p,Al}\Delta T_{max}e^{-t^2/\tau^2} \tag{6}$$

where τ is the e^{-1} laser pulse width (6 ns), ΔT_{max} is the peak temperature change, k_{Al}, ρ_{Al}, L_{Al}, and $c_{p,Al}$ is the aluminum thermal conductivity, density, thickness, and heat capacity, respectively. The silicon wafer is assumed to be semi-infinite since the thermal diffusion time through the silicon is much larger than the microsecond time scale of the measurement.

The interfaces between the aligned CNT film and both the metal film and the SiO_2 film provide four boundary conditions,

$$q''_{Al\text{-}CNT} = (R''_{CNT\text{-}Pd,eff})^{-1}(T_{Al}(L_{Al}) - T_{CNT}(0)) = -k_{Al}\left.\frac{\partial T_{Al}}{\partial x}\right|_{L_{Al}} \tag{7}$$

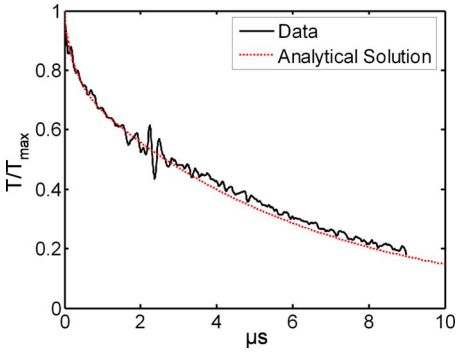

Fig. 3 Typical thermal response trace data for a particular measurement (solid) for the 28 μm sample along with the best-fit analytical solution evaluated with the average best-fit parameters summarized in Table 1 below (dashed). The data show two characteristic decay time scales during the measurement: the initial rapid decay lasting ~0.5 μs followed by a longer decay lasting ~4 μs.

$$-k_{Al}\left.\frac{\partial T_{Al}}{\partial x}\right|_{x_{Al}=L_{Al}} = -k_{CNT,eff}\left.\frac{\partial T_{CNT}}{\partial x}\right|_{x_{CNT}=0} \tag{8}$$

$$q''_{CNT\text{-}SiO_2} = (R''_{CNT\text{-}SiO_2,eff})^{-1}(T_{CNT}(L_{CNT}) - T_{SiO_2}(0)) = -k_{SiO_2}\left.\frac{\partial T_{SiO_2}}{\partial x}\right|_{x_{SiO_2}=0} \tag{9}$$

$$-k_{CNT,eff}\left.\frac{\partial T_{Al}}{\partial x}\right|_{x_{CNT}=L_{CNT}} = -k_{SiO_2}\left.\frac{\partial T_{SiO_2}}{\partial x}\right|_{x_{SiO_2}=0} \tag{10}$$

where $k_{CNT,eff}$ is the area-averaged CNT thermal conductivity and $R''_{CNT\text{-}Pd,eff}$ and $R''_{CNT\text{-}SiO_2,eff}$ are the area-averaged contact resistances between the CNTs and the palladium adhesion layer and oxide films, respectively. We define the resistance at the metallized contact as $R''_{CNT\text{-}Pd,eff}$ because the nanotubes directly contact the palladium adhesion layer underlying the aluminum film. An inverse Fourier transform converts the frequency domain solution back to the time domain, which we then fit to the experimental thermal data using a least squares curve fit algorithm.

Fitting the thermal model to the measured data is an inverse heat transfer analysis requiring the simultaneous fit of the four unknown parameters in the governing equations: $k_{CNT,eff}$, $C_{CNT,eff}$ (through $\alpha_{CNT,eff}$), $R''_{CNT\text{-}Pd,eff}$, and $R''_{CNT\text{-}SiO_2,eff}$. The impact and sensitivity of variation in each parameter on the shape of the thermal response is unique and evident at different time scales because each appears in a unique way though the governing equations (Eqs. (3) and (7)–(10)) and is localized in the vertical direction. Since the measurement is capable of resolving time scales below the thermal diffusion time through the CNT film, these properties can be accurately and individually resolved. We verified this capability by a mathematically rigorous parametric variation study of the best-fit solution of the heat diffusion equation to the experimental data.

Results and Discussion

Figure 3 shows a representative thermal response for the sample along with the least squares best-fit analytical solution evaluated with the average of the extracted properties. Nine measurements at multiple locations on the samples and at multiple laser pump powers were individually fit to the analytical heat diffusion model, and the effective parameters were averaged to produce the results shown in Table 1. Table 1 shows the corresponding rms error in the data, which is dominated by variations

Table 1 Best-fit values averaged from multiple measurements of $C_{CNT,eff}$, $R''_{CNT\text{-}Pd,eff}$, $R''_{CNT\text{-}SiO_2,eff}$, and $k_{CNT,eff}$ for the 28 μm thick sample along with their associated uncertainty. The uncertainty is calculated from the rms variation in extracted parameters individually fitted to multiple measurements.

Parameter	Average result	Uncertainty (%)
$C_{CNT,eff}$	5.2 kJ m^{-3} K^{-1}	12%
$R''_{CNT\text{-}Pd,eff}$	2.9 m^2 K^1 MW^{-1}	21%
$R''_{CNT\text{-}SiO_2,eff}$	9.1 m^2 K^1 MW^{-1}	31%
$k_{CNT,eff}$	>8 W m^{-1} K^{-1}	—

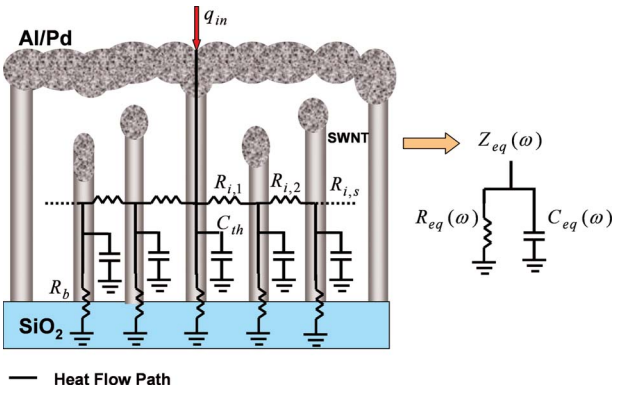

Fig. 4 Schematic illustrating the hypothesis that a subset of the CNTs is in good thermal contact with the porous and discontinuous evaporated film. The data suggest that the overwhelming majority of the heat transport is brought about by longer tubes that fully contact the metal film. We use a thermal circuit model to account for lateral thermal transport in the CNT film. The heat flows into the central tube that is in thermal contact with the metal film and then flow laterally through the intertube coupling resistance to surrounding tubes. We reduce the thermal network to a frequency dependant parallel equivalent *RC* thermal circuit, which is what is experimentally measured.

in the shape of the trace and uncertainty due to amplitude noise. Errors due to the sensitivity of the least squares fitting algorithm applied to a single thermal response trace generally contribute less than 10% error for each parameter.

An estimate of the thermal diffusion time through the CNT film qualitatively explains the particular shape of the thermal trace in Fig. 3, which displays an initial rapid decay lasting <0.5 μs followed by a second, slower decay lasting ~4 μs. The characteristic thermal diffusion time through the SWNT film is given by $t_{diff}=L^2_{CNT}/\alpha_{CNT}$, where $L_{CNT}=28$ μm is the thickness of the CNTs and α_{CNT} is the individual CNT thermal diffusivity. From the measurement of $c_p=660$ mJ g^{-1} K^{-1} by Hone et al. [37] and the CNT unit cell volume, we estimate $C_{v,a}$ to be 1.5 MJ m^{-3} K^{-1}, which is the volumetric heat capacity for an individual SWNT compatible with the area definition, $A_a=\pi db$. Combined with a value of $k_{CNT}=3600$ W m^{-1} K^{-1} [4], $\alpha_{CNT}\sim 2.4\times10^{-3}$ m^2 s^{-1} and $t_{diff}=0.33$ μs, which is in reasonable agreement with the time scale for the initial rapid decay demonstrated by the data. Consequently, the initial decay rate for times less than t_{diff} is relatively insensitive to the CNT-oxide contact resistance. A rigorous parametric variation study of the fitting parameters in the analytical model verified that the initial rapid decay rate is dominated by $R''_{CNT\text{-}Pd,eff}$ and that $R''_{CNT\text{-}SiO_2,eff}$ dominates the long-time decay characteristics.

Due to the large effective thermal interface resistances in the structure, the measurement only yields a potential lower bound of ~8 W m^{-1} K^{-1} for the area-averaged thermal conductivity of the array, which corresponds to a total CNT resistance below ~3.5 m^2 K MW^{-1}. No solution fit was attainable for thermal conductivities lower than this value, and the fit of the remaining parameters to the data trace was insensitive to conductivities at and above this value.

The data in Table 1 show that the effective CNT heat capacity is quite low, even accounting for the nanotube film porosity. Because the heat capacity is expected to be relatively insensitive to interface effects, the data suggest that only a fraction of the CNTs contribute to the volumetric specific heat. The ratio of the measured effective heat capacity to the volumetric heat capacity of an individual tube ($f_{eff,C}$) provides an estimate of the effective volume fraction of CNTs contributing to the thermal capacity in the structure,

$$f_{eff,C}=\frac{C_{CNT,eff}}{C_{v,a}}=0.0035 \tag{11}$$

which includes the contributions to the porosity occurring within an individual tube and does not require precise knowledge of the SWNT diameter. Based on an estimated average nanotube diameter of 1.3 nm, $f_{eff,C}$ corresponds to the number density of 2.5 $\times10^{15}$ m^{-2}, which is much less than the prior estimate of the SWNT yield based on the catalyst preparation conditions. A thermal model for transport within the nanotube structure presented in the subsequent section concludes that the effective volume fraction of CNTs contributing to the thermal resistance in the CNT array ($f_{eff,R}$) is nearly identical to $f_{eff,C}$. Scaling the lower bound on the area-averaged effective CNT thermal conductivity by this fraction provides an estimate of ~2300 W m^{-1} K^{-1} for the lower bound on the intrinsic conductivity of an individual SWNT measured in this study.

Since the CNT thermal resistance is small in comparison to the interface contributions, the total effective thermal resistance of the SWNT structure is determined by the sum of the boundary resistances to be $R''_{SWNT,tot}=12$ m^2 K MW^{-1}. This value is comparable to the values of 12–23 m^2 K MW^{-1} [20,22,38] for aligned MWNT array structures measured in prior work. The lower performance of the MWNT arrays may be due to the decrease in conformability of the shorter nanotubes, an increase in surface roughness of the MWNT arrays, or a significantly lower intrinsic resistance of MWNTs. Although the contact between the SWNT and the metal is probably much stronger than the van der Waal dominated contact in the MWNT experiments, the use of pressure most likely increased the number of tubes contacting the interface in the MWNT experiments.

Thermal Model for Conduction in CNT Films

In this section, we propose a hypothesis for the nanoscale SWNT-metal contact geometry that aims to explain the unexpectedly low values of the effective heat capacity and large interface resistances presented in Table 1. Related to this hypothesis, we develop an approximate thermal model of heat transport within the CNT film with the purpose of understanding the relationship between the effective volume fraction of tubes that contribute to the heat capacity and those that contribute to the thermal resistance within the CNT array. Through this understanding, we can estimate the intrinsic thermal contact resistance between an individual SWNT and a metal film from the measured data.

Since the aluminum film (Fig. 1(*c*)) is porous with its nominal thickness of 160 nm being comparable to the 60 nm rms CNT surface roughness, we believe that incomplete contact between the SWNTs and the metal film reduces the CNT volume fraction that contributes to heat conduction significantly below the 12 vol % of CNTs estimated from the catalyst preparation conditions. Figure 4 schematically illustrates our belief that the uneven CNT surface topography due to the variation in SWNT heights, combined with

the porosity of the metal film, causes the metal to make poor contact, particularly with the shorter nanotubes in the array.

To understand how the hypothesized contact geometry relates to the film thermal properties, we suggest a simple geometric model for the incomplete CNT-metal thermal contact in which we consider one individual SWNT that is in contact with the metal film and assume that the surrounding tubes are not in contact with the metal film. We will assume that heat flows into the central tube and can then couple to the surrounding tubes through an intertube coupling resistance R_i'' (m^2 K W^{-1}) (defined on the CNT perimeter area $A_p = \pi d L_{\mathrm{CNT}}$). Included in the inter-tube coupling resistance are all possible thermal transport channels, such as conduction, radiation, and occasional CNT-CNT contact between two aligned CNTs. Equating a thermal network model (Fig. 4) of heat transfer within the CNT array to an equivalent parallel effective thermal capacitance and resistance of the SWNT yields the experimentally measured effective thermal properties.

Because the interface resistance is much larger than the intrinsic SWNT resistance, we model the thermal impedance of each nanotube as a lumped thermal capacitor in parallel with a thermal boundary resistance R_b (K W^{-1}) between the SWNT and the oxide layer. The total complex thermal impedance of an individual CNT is

$$Z_{\mathrm{CNT}} = \frac{Z_C Z_b}{Z_C + Z_b} \tag{12}$$

where

$$Z_b = R_b \tag{13}$$

$$Z_C = \frac{1}{i\omega C_{\mathrm{th}}} \tag{14}$$

where $C_{\mathrm{th}} = C_{v,a} \pi d b L_{\mathrm{CNT}}$ is the total heat capacity of an individual tube. The total effective admittance of the CNT network is given by

$$\frac{1}{Z_{\mathrm{eff}}} = \frac{1}{Z_{\mathrm{CNT}}} + \frac{1}{Z_{s,\mathrm{eff}}} \tag{15}$$

where $Z_{s,\mathrm{eff}}$ is the total thermal impedance contribution from the surrounding neighboring tubes calculated below. Equating the admittance of Eq. (15) to the admittance of the equivalent parallel *RC* thermal circuit,

$$\frac{1}{Z_{\mathrm{eq}}} = \frac{1}{R_{\mathrm{eq}}(\omega)} + i\omega C_{\mathrm{th,eq}}(\omega) \tag{16}$$

yields

$$R_{\mathrm{eq}}(\omega) = \frac{1}{\mathrm{Re}\left(\frac{1}{Z_{\mathrm{eff}}}\right)} \tag{17}$$

$$C_{\mathrm{th,eq}}(\omega) = \frac{1}{\omega}\,\mathrm{Im}\left(\frac{1}{Z_{\mathrm{eff}}}\right) \tag{18}$$

A frequency-weighted average based on a representative thermal spectrum of the analytical solution of the metal temperature field yields the total R_{eq} and $C_{\mathrm{th,eq}}$ for the SWNT in contact with the metal film

$$R_{\mathrm{eq}} = \frac{\int_\omega R_{\mathrm{eq}}(\omega) X(\omega) d\omega}{\int_\omega X(\omega) d\omega} \tag{19}$$

$$C_{\mathrm{th,eq}} = \frac{\int_\omega C_{\mathrm{th,eq}}(\omega) X(\omega) d\omega}{\int_\omega X(\omega) d\omega} \tag{20}$$

where $X(\omega)$ is the amplitude of the Fourier transform of the metal thermal response.

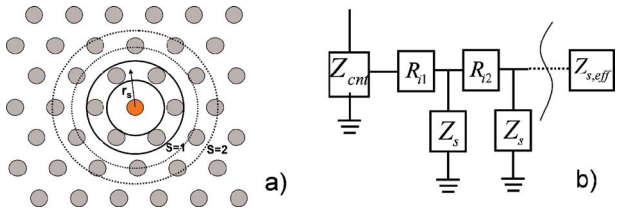

Fig. 5 (*a*) Schematic top view of a CNT in a close-pack arrangement grouped into concentric shells of neighboring tubes to calculate the effective impedance of the series of neighboring tubes, as assumed in the model. (*b*) Block diagram of impedance network modeling the linking of neighboring shells by an intershell thermal resistance.

We calculate the total impedance of the surrounding neighboring tubes, $Z_{s,\mathrm{eff}}$, by assuming a simple close-pack arrangement of the CNTs shown schematically in Fig. 5(*a*). Around the central tube contacting the metal film, we separate by the average CNT spacing the surrounding noncontacting tubes into concentric "nearest neighbor" shells. The intertube coupling resistance R_i'' links the total thermal impedance of each shell in the network (Fig. 5(*b*)).

From the CNT geometric arrangement, the total impedance of the parallel n_s tubes in the *s*th shell from the central tube is

$$Z_{\mathrm{CNT},s} = \frac{Z_{\mathrm{CNT}}}{n_s} \tag{21}$$

where the number of tubes in the *s*th shell is

$$n_s = 8s\sqrt{\frac{\pi\phi}{2\sqrt{3}}} \tag{22}$$

and where *s* is the shell label (1, 2, 3, …) and ϕ is the volume fraction ($\sim 12\%$). The total resistance between the *s*th and the $(s-1)$th, shell in terms of R_i'' is

$$R_{i,s} = R_i''\left(\frac{1}{A_{\mathrm{inner}}} + \frac{1}{A_{\mathrm{outer}}}\right) = \frac{R_i''}{\pi d L\sqrt{\frac{32\pi\phi}{\sqrt{3}}}}\left(\frac{1}{s} + \frac{1}{s-1}\right) \tag{23}$$

Combining Eqs. (21) and (23), yields the recursive relation for the total effective impedance of $Z_{s,\mathrm{eff}}$ and all shells beyond

$$Z_{s,\mathrm{eff}} = R_{i,s} + \frac{Z_{\mathrm{CNT},s} Z_{s+1,\mathrm{eff}}}{Z_{\mathrm{CNT},s} + Z_{s+1,\mathrm{eff}}} \tag{24}$$

which gives $C_{\mathrm{th,eq}}$ and R_{eq} through Eq. (15) and the subsequent relations.

In Fig. 6, we show the dependence of $C_{\mathrm{th,eq}}$ and R_{eq}, normalized to the capacitance $C_{\mathrm{th,CNT}}$ and resistance R_b of an individual tube, on R_i''. Figure 6 shows that C_{eff} and R_{eq} are essentially equivalent to the individual tube values for $R_i'' > 10^{-3}$ m^2 K W^{-1}, indicating that lateral conduction within the CNT array is negligible in this regime. Using two vertically aligned MWNT arrays pressed together in an opposing configuration, Hu et al. [39] measured $R_i'' = 1.4$ m^2 K W^{-1}, which is very large. While interpenetrating MWNTs pressed in an opposed geometry is a variant of the aligned SWNT geometry of this study, the similarity in thermal transport in aligned independent nanostructures allows for a sensible comparison. Owing to an increased CNT-CNT contact due to mechanical deformation, the MWNT intertube coupling resistance presumably provides a lower bound for the SWNT case.

Recent work using classic molecular dynamics simulations to investigate the dependence of the intertube thermal contact resistance between two aligned SWNTs on the distance between the CNT walls show that for distances larger than ~ 1.3 nm, the intertube thermal resistance is extraordinarily large

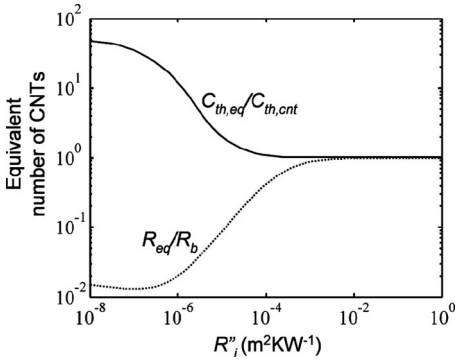

Fig. 6 The effective thermal capacity $C_{th,eq}$, and thermal resistance, R_{eq} due to intertube coupling effects normalized to that of an individual tube as a function the intertube coupling resistance R''_i

($>10^{-4}$ m^2 K W^{-1}) [40]. That the intertube resistance predicted by the simulations in Ref. [40] agrees reasonably with measurements of the interfacial thermal resistance between SWNTs and octane [23] suggests that the simulations capture the essential nanoscale physics and that a phenomenon such as near field radiation transfer is insignificant in this analysis. Based on the prior data and simulations, we believe that intertube coupling effects are insignificant in the analysis in this work. Thus, the effective thermal properties are entirely determined by the tubes that are in thermal contact with the metal film, and the tubes in poor thermal contact contribute negligibly. If intertube transport were significant, then the number of tubes that contribute to volumetric heat capacity would differ from the number of tubes that contribute to the thermal resistance and contact resistance.

If intertube coupling is negligible, the effective volume fraction of tubes contributing to conduction is nearly identical to the effective volume fraction contributing to the heat capacity. Thus,

$$f_{\text{eff},R} \approx f_{\text{eff},C} = 0.0035 \tag{25}$$

The calculation of these results exploits the directly measured volumetric heat capacity and does not depend on the precise knowledge of the true CNT film porosity, which is challenging to directly measure. This small effective volume fraction contributing to thermal transport, which we attribute to poor contact geometry, provides an explanation for the extraordinarily large thermal boundary resistances observed in most nanotube arrays.

Additionally, if intertube coupling effects are negligible, the volume fraction of tube contribution to conduction and interface resistance is the same. Scaling the area-averaged interface resistances by $f_{\text{eff},R}$ yields a value of 10 m^2 K GW^{-1} for the individual CNT-Pd contact resistance and 32 m^2 K GW^{-1} for the individual CNT-SiO_2 contact resistance, consistent with the area definition A_a. We believe that the two additional interfaces with the catalyst and SiO_2 at the base of the CNTs explain why $R''_{\text{CNT-SiO}_2}$ is about three times larger than $R''_{\text{CNT-Pd}}$.

It is useful to compare the extracted results of the intrinsic CNT-metal contact resistance with both other experimental studies and theoretical calculations. Utilizing Joule self-heating of a MWNT on a metal substrate, Kim et al. [10] measured the CNT-metal contact resistance to be 29 m^2 K^1 GW^{-1}, based on the area $A=dL_{\text{CNT}}$, where $d=14$ nm is the diameter and $L_{\text{CNT}}=1$ μm is the contact length. The reasonable agreement of Ref. [10] with those presented in this paper suggests that the mechanisms of thermal transport between a metal deposited on the end of a CNT and a CNT lying on a metal substrate may be similar.

We can provide an approximate lower bound for CNT-Pd contact resistance using the acoustic mismatch (AMM) theory of boundary resistance, reviewed in Schwartz and Pohl [41], in which phonon transport across a boundary is treated analogously to acoustic impedance mismatches. The AMM theory has been developed and applied to thermal interfaces between three dimensional materials, with insufficient development for interfaces between low dimensional structures of possibly differing dimensionalities.

A proper characterization of the nanoscale interface is critical because the complicated and ambiguous nanoscale geometry strongly dictates the mathematical structure of the AMM calculation. Although a SWNT is often treated as a quasi-1D structure, its interface with a metal includes 2D and 3D aspects. We make the approximation that the nanotubes have a quasi-2D isotropic "flat-sheet" geometry since nanotubes behave much like a 2D graphene sheet due to the strong excitation of the phonon subbands at room temperature [37]. We consider one longitudinal and two transverse acoustic polarization branches as well as model the Pd as an isotropic 2D medium. We derive the heat flux for a given temperature drop across the 2D boundary analogously to a 3D medium as in Refs. [41,42] to be

$$\dot{q}'_{\text{CNT-Pd}} = \left(\frac{1}{2\pi}\right)^2 \left(\frac{k_b T_{\text{CNT}}}{\hbar}\right)^3 \sum_{s=\text{pol}} \int_{-\pi/2}^{\pi/2} \alpha_{\text{CNT-Pd},s}(\theta) \left(\frac{\hbar}{c_s}\right) \cos(\theta) d\theta \times \int_0^{\theta_{d,\text{Pd}}/T_{\text{Pd}}} x^3 \left[\frac{1}{e^{\left(x\frac{T_{\text{CNT}}}{T_{\text{Pd}}}\right)}} - \frac{1}{e^x}\right] dx \tag{26}$$

where $\theta_{d,\text{Pd}} \sim 250$ K is the Debye temperature of the palladium, T_{CNT} and T_{Pd} are the temperatures of the CNT and Pd sides of the boundary, respectively, and $\alpha_{\text{CNT-Pd},s}(\theta)$ is the transmission coefficient computed using the AMM approximation given in Ref. [41],

$$\alpha_{\text{CNT-Pd},s}(\theta) = \frac{4\dfrac{(\rho_{\text{Pd}} c_{\text{Pd},s})}{(\rho_{\text{CNT}} c_{\text{CNT},s})}}{\left[\dfrac{(\rho_{\text{CNT}} c_{\text{CNT},s})}{(\rho_{\text{CNT}} c_{\text{CNT},s})} + \dfrac{\cos(\theta_{\text{Pd}})}{\cos(\theta_{\text{CNT}})}\right]^2} \tag{27}$$

where ρ_i is the density of material i, $c_{i,s}$ is the acoustic velocity of polarization s in material i, and θ_i is the phonon angle of incidence in side i. Computing the heat flux from the CNT side avoids critical cone considerations since it has the higher phonon velocities [42]. Assuming elastic boundary scattering with no mode conversion, the integral in Eq. (26) is limited by the lower Debye temperature (Pd) since no modes at higher frequency can be transmitted into the Pd.

From Eq. (26), the boundary resistance is defined as

$$R''_{\text{AMM}} = \frac{(T_{\text{CNT}} - T_{\text{Pd}})b}{\dot{q}'_{\text{CNT-Pd}}} \tag{28}$$

which upon numerical evaluation gives $R''_{\text{AMM}}=3.1$ m^2 K^1 GW^{-1} and is consistent with the area $A_a=\pi db$ in which the phonons in the CNT are confined. The AMM calculation predicts a boundary resistance 3.2 times lower than the extracted value for the SWNT-Pd contact, which is rather reasonable considering that AMM predictions are usually much larger at room temperature [41]. Typically, the AMM theory only applies at low temperature where the phonon wavelength is much larger that the interface roughness. However, we believe that the AMM model predicts reasonable results because the Debye temperature of the CNTs is much higher than room temperature ($\theta_{d,\text{CNT}} \sim 2500$ K), so the calculations are in the "low temperature" regime when performed from the CNT side. Also, the nanotube-metal contact is atomistic; thus, conventional surface roughness considerations in phonon transport are poorly defined and inapplicable.

The consistency of the experimental results with the AMM predictions indicates that the intrinsic conduction between an individual CNT and a metal film approaches fundamental physical limits. Thus, increasing the number of CNT-substrate contacts is

the most promising approach for improving the thermal performance of CNT-based interface materials. Moreover, the discrepancy between theory and the measured data merits future theoretical analysis, possibly considering more detailed modeling of the nanoscale dimensional effects and transport at the interface between the quasi-1D CNT and the 3D metal film.

Summary and Conclusions

This paper studies the room temperature thermal properties of metalized vertically aligned SWNTs using a nanosecond thermoreflectance technique. We measure the total thermal resistance of the TIM to be $R''_{\text{eff,tot}}=12\ \text{m}^2\ \text{K MW}^{-1}$, which we determine to be dominated by the interface resistance and not the thermal conductivity of the CNTs themselves. Images of the metal film and the CNT surface topography suggest a model for the CNT-metal contact, whereby only a subset of the CNTs are actually responsible for the thermal transport. The results show that the effective volume fraction of SWNTs contributing to thermal transports is 0.35%, which is much less than the estimation of the true volume fraction of ~12% from the catalyst deposition process. Based on the effective volume fraction, the intrinsic thermal resistance for an individual SWNT-Pd contact is $R''_{\text{CNT-Pd},a}=10\ \text{m}^2\ \text{K GW}^{-1}$ (based on the annular area, $A_a=\pi db$), which is in reasonable agreement with the upper limit predictions of the AMM theory. These results suggest that increasing the number of CNT-substrate contacts can potentially reduce the total thermal resistance of a SWNT array to less than $1\ \text{m}^2\ \text{K MW}^{-1}$. Future work toward developing practical CNT based TIMs needs to address the CNT contact geometry as well as characterize the lateral mechanical compliance of aligned nanotube arrays and their effect on the contact geometry and thermal transport, particularly during thermal cycling.

Acknowledgment

The authors gratefully acknowledge the financial support from SRC (2003-NJ-1064), DARPA (N6001-04-8916), MARCO Interconnect Focus Center, and a NSF NIRT (Award No. 1058163-1-QAXYZ). M.A.P. thanks the Stanford Graduate Fellowship program.

Nomenclature

A_a = annular area of individual CNTs, m^2
A_d = cross-sectional area of individual CNTs, m^2
b = thickness of CNT annular area, m
c_s = CNT acoustic speed of polarization s, m s^{-1}
c_p = heat capacity, $\text{J kg}^{-1}\ \text{K}^{-1}$
$C_{\text{CNT,eff}}$ = area-averaged effective volumetric heat capacity, $\text{J m}^{-3}\ \text{K}^{-1}$
C_{th} = thermal capacity, J K^{-1}
C_{tr} = thermoreflectance coefficient, K^{-1}
$C_{v,a}$ = volumetric heat capacity of individual SWNTs based on A_a, $\text{J m}^{-3}\ \text{K}^{-1}$
$C_{v,d}$ = volumetric heat capacity of individual SWNTs based on A_d, $\text{J m}^{-3}\ \text{K}^{-1}$
d = CNT diameter, m
$R''_{\text{CNT-Pd}}$ = individual Pd-CNT contact boundary resistance, $\text{m}^2\ \text{K W}^{-1}$
$R''_{\text{CNT-SiO}_2}$ = individual CNT-SiO_2 contact boundary resistance, $\text{m}^2\ \text{K W}^{-1}$
$R_{\text{CNT-Pd,eff}}$ = area-averaged effective Pd-CNT contact boundary resistance, $\text{m}^2\ \text{K W}^{-1}$
$R''_{\text{CNT-SiO}_2\text{,eff}}$ = area-averaged effective CNT-SiO_2 contact boundary resistance, $\text{m}^2\ \text{K W}^{-1}$
k_{Al} = thermal conductivity of aluminum film, $\text{W m}^{-1}\ \text{K}^{-1}$
$k_{\text{CNT,eff}}$ = effective area-averaged thermal conductivity of nanotube film, $\text{W m}^{-1}\ \text{K}^{-1}$
k_{SiO_2} = thermal conductivity of oxide layer, $\text{W m}^{-1}\ \text{K}^{-1}$
k_B = Boltzmann constant $=1.38\times10^{-23}\ \text{J K}^{-1}$
L_{Al} = thickness of aluminum, m
L_{CNT} = length of a CNT, m
n_s = number of CNTs in shell s
q'' = heat flux, W m^{-2}
R = reflectivity
R_b = total thermal boundary resistance of nanotube, K W^{-1}
R''_b = CNT thermal boundary resistance, $\text{m}^2\ \text{K W}^{-1}$
R''_{CNT} = CNT thermal resistance, $\text{m}^2\ \text{K W}^{-1}$
R_{eff} = effective resistance of an individual CNT including intertube coupling, K W^{-1}
R''_i = intertube thermal coupling resistance, $\text{m}^2\ \text{K W}^{-1}$
$R_{i,s}$ = shell s intertube thermal resistance, K W^{-1}
s = shell number
t = time, s
T_i = temperature of the ith material, K
x = position, m
Z_b = thermal interface impedance of individual CNT-substrate contacts K W^{-1}
Z_C = thermal capacitance impedance of individual SWNTs, K W^{-1}
Z_{CNT} = total SWNT thermal impedance, K W^{-1}
Z_{eff} = effective thermal impedance of CNT thermal network model, K W^{-1}
Z_{eq} = thermal impedance of an equivalent parallel RC thermal network, K W^{-1}
$Z_{s,\text{eff}}$ = total effective thermal impedance of s concentric shells of CNTs, K W^{-1}
Z_s = total thermal impedance of shell s, K W^{-1}

Greek Symbols

α_i = thermal diffusivity of the ith material, $\text{m}^2\ \text{s}^{-1}$
$\alpha_{\text{CNT-Pd}}$ = phonon boundary transmission coefficient
θ_i = Fourier transform of the temperature of the ith material, K
θ_d = Debye temperature, K
ρ = density, kg m^{-3}
τ = laser temporal pulse width, s
ϕ = volume fraction
ω = frequency, rad/s

References

[1] Osman, M. A., and Srivastava, D., 2001, "Temperature Dependence of the Thermal Conductivity of Single-Wall Carbon Nanotubes," Nanotechnology, **12**, pp. 21–21.
[2] Berber, S., Kwon, Y.-K., and Tománek, D., 2000, "Unusually High Thermal Conductivity of Carbon Nanotubes," Phys. Rev. Lett., **84**, pp. 4613–4616.
[3] Maruyama, S., 2003, "A Molecular Dynamics Simulation of Heat Conduction of a Finite Legth Single-Walled Carbon Nanotube," Microscale Thermophys. Eng., **7**, pp. 41–50.
[4] Pop, E., Mann, D., Wang, Q., Goodson, K., and Dai, H., 2006, "Thermal Conductance of an Individual Single-Wall Carbon Nanotube Above Room Temperature," Nano Lett., **6**(1), pp. 96–100.
[5] Lukes, J. R., and Zhong, H., 2007, "Thermal Conductivity of Individual Single-Wall Carbon Nanotubes," ASME J. Heat Transfer, **129**(6), pp. 705–716.
[6] Padgett, C. W., and Brenner, D. W., 2004, "Influence of Chemisorption on the Thermal Conductivity of Single-Wall Carbon Nanotubes," Nano Lett., **4**(6), pp. 1051–1053.
[7] Mingo, N., and Broido, D. A., 2005, "Length Dependence of Carbon Nanotube Thermal Conductivity and the 'Problem of Long Waves'," Nano Lett., **5**(7), pp. 1221–1225.
[8] Mingo, N., and Broido, D. A., 2005, "Carbon Nanotube Ballistic Thermal Conductance and Its Limits," Phys. Rev. Lett., **95**(9), pp. 096105.
[9] Pan, R., Xu, Z., Zhu, Z., and Wang, Z., 2007, "Thermal Conductivity of Functionalized Single-Wall Carbon Nanotubes," Nanotechnology, **18**(28), p. 285704.
[10] Kim, P., Shi, L., Majumdar, A., and McEuen, P. L., 2001, "Thermal Transport Measurements of Individual Multiwalled Nanotubes," Phys. Rev. Lett.,

87(21), p. 215502.
[11] Fujii, M., Zhang, X., Xie, H., Ago, H., Takahashi, K., Ikuta, T., Abe, H., and Shimizu, T., 2005, "Measuring the Thermal Conductivity of a Single Carbon Nanotube," Phys. Rev. Lett., **95**, p. 065502.
[12] Hone, J., Llaguno, M. C., Nemes, N. M., and Johnson, A. T., 2000, "Electrical and Thermal Transport Properties of Magnetically Aligned Single Wall Carbon Nanotube Films," Appl. Phys. Lett., **77**, pp. 666–668.
[13] Yi, W., Lu, L., Dian-lin, Z., Pan, Z. W., and Xie, S. S., 1999, "Linear Specific Heat of Carbon Nanotubes," Phys. Rev. B, **59**, pp. R9015–R9018.
[14] Shenogin, S., Xue, L., Ozisik, R., Keblinski, R., and Cahill, D., 2004, "Role of Thermal Boundary Resistance on the Heat Flow in Carbon-Nanotube Composites," J. Appl. Phys., **95**, pp. 8136–8144.
[15] Xue, Q. Z., 2006, "Model for the Effective Thermal Conductivity of Carbon Nanotube Composites," Nanotechnology, **17**(6), pp. 1655–1660.
[16] Choi, S. U. S., Zhang, Z. G., Yu, W., Lockwood, F. E., and Grulke, E. A., 2001, "Anomalous Thermal Conductivity Enhancement in Nanotube Suspensions," Appl. Phys. Lett., **79**, pp. 2252–2254.
[17] Biercuk, M. J., Llaguno, M. C., Radosavljevic, M., Hyun, J. K., Johnsond, A. T., and Fischer, J. E., 2002, "Carbon Nanotube Composites for Thermal Management," Appl. Phys. Lett., **80**, pp. 2767–2769.
[18] Guthy, C., Du, F., Brand, S., Winey, K. I., and Fischer, J. E., 2007, "Thermal Conductivity of Single-Walled Carbon Nanotube/PMMA Nanocomposites," ASME J. Heat Transfer, **129**(8), pp. 1096–1099.
[19] Hu, X., Jiang, L., and Goodson, K. E., 2004, "Thermal Conductance Enhancement of Particle-Filled Thermal Interface Materials Using Carbon Nanotube Inclusions," *Proceedings of the Intersociety Conference on Thermal and Thermo-Mechanical Phenomena in Electronic Systems*, pp. 63–69.
[20] Hu, X. J., Padilla, A. A., Xu, J., Fisher, T. S., and Goodson, K. E., 2006, "3-Omega Measurements of Vertically Oriented Carbon Nanotubes on Silicon," ASME J. Heat Transfer, **128**(11), pp. 1109–1113.
[21] Yang, D. J., Zhang, Q., Chen, G., Yoon, S. F., Ahn, J., Wang, S. G., Zhou, Q., Wang, Q., and Li, J. Q., 2002, "Thermal Conductivity of Multiwalled Carbon Nanotubes," Phys. Rev. B, **66**, p. 165440.
[22] Tong, T., Zhao, Y., Delzeit, L., Kashani, A., Meyyappan, M., and Majumdar, A., 2007, "Dense Vertically Aligned Multiwalled Carbon Nanotube Arrays as Thermal Interface Materials," IEEE Trans. Compon. Packag. Technol., **30**(1), pp. 92–100.
[23] Huxtable, S. T., Cahill, D. G., Shenogin, S., Xue, L., Ozisik, R., Barone, P., Usrey, M., Strano, M. S., Siddons, G., Shim, M., and Keblinski, P., 2003, "Interfacial Heat Flow in Carbon Nanotube Suspensions," Nat. Mater., **2**(11), pp. 731–734.
[24] Zhang, G., Mann, D., Zhang, L., Javey, A., Li, Y., Yenilmez, E., Wang, Q., McVittie, J. P., Nishi, Y., Gibbons, J., and Dai, H., 2005, "Ultra-High-Yield Growth of Vertical Single-Walled Carbon Nanotubes: Hidden Roles of Hydrogen and Oxygen," Proc. Natl. Acad. Sci. U.S.A., **102**, pp. 16141–16145.
[25] Chu, D., Touzelbaev, M., Babin, S., Pease, R. F., and Goodson, K. E., 2001, "Thermal Conductivity Measurements of Thin-Film Resist," J. Vac. Sci. Technol. B, **19**, pp. 2874–2877.
[26] Kading, O. W., Skurk, H., and Goodson, K. E., 1994, "Thermal Conduction in Metallized Silicon-Dioxide Layers on Silicon," Appl. Phys. Lett., **65**(13), pp. 1629–1631.
[27] Smith, A., Hostetler, D., and Norris, P., 2000, "Thermal Boundary Resistance Measurements Using a Transient Thermoreflectance Technique," Microscale Thermophys. Eng., **4**, pp. 51–60.
[28] Stoner, R., and Maris, H., 1993, "Kapitza Conductance and Heat Flow Between Solids at Temperature From 50 to 300 K," Phys. Rev. B, **48**, pp. 16373–16387.
[29] Paddock, C. A., and Eesley, G. L., 1986, "Transient Thermoreflectance From Thin Metal Films," J. Appl. Phys., **60**, pp. 285–290.
[30] Schoenlein, R. W., Lin, W. Z., Fujimoto, J. G., and Eesley, G. L., 1987, "Femtosecond Studies of Nonequilibrium Electronic Processes in Metals," Phys. Rev. Lett., **58**(16), pp. 1680–1683.
[31] Elsayed-Ali, H. E., Norris, T. B., Pessot, M. A., and Mourou, G. A., 1987, "Time-Resolved Observation of Electron-Phonon Relaxation in Copper," Phys. Rev. Lett., **58**(12), pp. 1212–1215.
[32] Ujihara, K., 1972, "Reflectivity of Metals at High Temperatures," J. Appl. Phys., **43**, pp. 2376–2383.
[33] Guidotti, D., and Wilman, J., 1991, "Novel and Nonintrusive Optical Thermometer," Appl. Phys. Lett., **60**, pp. 524–526.
[34] Clemens, B., Eesley, G., and Paddock, C., 1988, "Time-Resolved Thermal Transport in Compositionally Modulated Metal Films," Phys. Rev. B, **37**, pp. 1085–1096.
[35] Bethe, H. A., 1944, "Theory of Diffraction by Small Holes," Phys. Rev., **66**, pp. 163–182.
[36] Jin, E. X., and Xu, X., 2005, "Radiation Transfer Through Nanoscale Apertures," J. Quant. Spectrosc. Radiat. Transf., **93**(1–3), pp. 163–173.
[37] Hone, J., Batlogg, B., Benes, Z., Johnson, A. T., and Fischer, J. E., 2000, "Quantized Phonon Spectrum of Single-Wall Carbon Nanotubes," Science, **289**(5485), pp. 1730–1733.
[38] Xu, J., and Fisher, T., 2004, "Thermal Contact Conductance Enhancement Using Carbon Nanotube Arrays," ASME Paper No. IMECE2004-60185.
[39] Hu, X. J., Panzer, M. A., and Goodson, K. E., 2007, "Infrared Microscopy Thermal Characterization of Opposing Carbon Nanotube Arrays," ASME J. Heat Transfer, **129**, pp. 91–93.
[40] Zhong, H., and Lukes, J. R., 2006, "Interfacial Thermal Resistance Between Carbon Nanotubes: Molecular Dynamics Simulations and Analytical Thermal Modeling," Phys. Rev. B, **74**(12), p. 125403.
[41] Schwartz, E., and Pohl, R., 1989, "Thermal Boundary Resistance," Rev. Mod. Phys., **61**, pp. 605–668.
[42] Phelan, P., 1998, "Application of Diffuse Mismatch Theory to the Prediction of Thermal Boundary Resistance in Thin-Film High-Tc Superconductors," ASME J. Heat Transfer, **120**, pp. 37–43.